JOURNAL OF GEOPHYSICAL RESEARCH, VOL. 115, A06211, doi:10.1029/2009JA014651, 2010

Time development of field-aligned currents, potential drops, and plasma associated with an auroral poleward boundary intensification

A. J. Hull,[1] M. Wilber,[1] C. C. Chaston,[1] J. W. Bonnell,[1] J. P. McFadden,[1] F. S. Mozer,[1] M. Fillingim,[1] and M. L. Goldstein[2]

Received 20 July 2009; revised 4 December 2009; accepted 28 January 2010; published 22 June 2010.

[1] We present a detailed case study of the plasma and fields measured by the Cluster spacecraft fleet at the high-altitude auroral zone (~3.5 R_E) across the plasma sheet boundary layer and into the polar cap. This event, which occurred during quiet geomagnetic conditions (Kp = 1^+, AE = 50 nT), is of particular interest in that Cluster provides measurements at key instances during the time development of a new large-scale auroral arc system. Central to the formation of the arc system is the depletion of ionospheric plasma through a region of small-scale, field-aligned currents having the properties of Alfvén waves. This depletion occurred prior to the growth of and ultimately bounded a well-defined equatorward moving, upward and downward current sheet pair. In association with the transverse scales approaching the electron inertial scale, the Alfvénic currents have amplitudes that appear to be attenuated subsequent to the formation of the cavity. Potential structures essentially time invariant over particle transit times (quasi-static) associated with the current pair are identified and observed to drive a poleward boundary intensification (PBI) identified in coincident IMAGE satellite far ultraviolet measurements. The PBI formed in association with a local thickening of the plasma sheet via the injection of new magnetospheric plasma, which may be the result of a bursty, patchy reconnection process. Estimates of the ionospheric equatorward velocity and thickness of the PBI are consistent with their ionospheric mapped cavity counterparts, suggesting that the motion and thickness are controlled by the plasma and electrodynamic features at or above the altitude sampled by Cluster. The magnitude of the upward and downward current region parallel potentials is correlated with the temperature of the newly injected electrons suggesting that the electron temperature is an important controlling factor. These novel observations indicate that quasi-static systems of field-aligned currents do form out of the highly dynamic Alfvénic region at the plasma sheet boundary layer, and perhaps suggest that the Alfvénic region can be the initial stage in the development of quasi-static systems. The observed time sequence of the currents is qualitatively similar to the expectations of transient response models of magnetospheric-ionospheric coupling, however, such models may need to be modified to account for the attenuation of electron inertial scale currents/Alfvén waves.

Citation: Hull, A. J., M. Wilber, C. C. Chaston, J. W. Bonnell, J. P. McFadden, F. S. Mozer, M. Fillingim, and M. L. Goldstein (2010), Time development of field-aligned currents, potential drops, and plasma associated with an auroral poleward boundary intensification, *J. Geophys. Res.*, *115*, A06211, doi:10.1029/2009JA014651.

1. Introduction

[2] The auroral acceleration region is an integral part of the magnetosphere-ionosphere electrodynamic system, and plays a key role in the transport of energy and particles between space and Earth. Processes occurring therein have received considerable attention over the past few decades, and can be organized into one (or more) of three broad regional categories: the upward current region, downward current region and Alfvénic region [see *Paschmann et al.*, 2003, chapter 4, and references therein]. In early studies of the upward and downward current acceleration regions a quasi-static interpretation of the data and models was often invoked to describe processes occurring therein. Namely, magnetospheric electrons are accelerated toward Earth via an electrostatic upward directed parallel electric field in

[1]Space Sciences Laboratory, University of California, Berkeley, California, USA.
[2]NASA Goddard Space Flight Center, Greenbelt, Maryland, USA.

0148-0227/10/2009JA014651

upward current regions. The parallel electric fields map to convergent perpendicular fields at higher altitudes yielding a "U-shaped" potential configuration. The U-shaped potential model is successful in explaining much of the equilibrium state of the upward current acceleration region, though modifications to incorporate a nonuniform altitude profile and corrugated (or fingering) structure [e.g., *Mozer and Hull*, 2001] may be required. A similar quasi-static U-shaped potential paradigm is often used to describe downward current regions.

[3] Although single spacecraft in situ studies, such as those based on the Freja, FAST, and Polar data sets, combined with theoretical modeling have solidified this understanding, the time development of the auroral acceleration region lacks a firm grounding in in situ observations. This is largely due to the fact that discrimination between spatial and temporal effects was problematic prior to the launch of the Cluster spacecraft quartet in 2000. With the exception of a few case studies [e.g., *Marklund et al.*, 2001, 2004; *Aikio et al.*, 2004, 2008], the time development of the plasma and fields within and above the acceleration region remains largely unstudied. Therefore important details of the time dependent processes that lead to the formation of parallel potential drops, and hence auroral arc formation, remain poorly understood. The studies by *Marklund et al.* [2001, 2004] used Cluster multipoint measurements primarily to study the temporal behavior of small-scale downward current regions at the polar cap boundary transition. They found that the downward current structures were quite transient, with the growth and decay of the size and intensity of the electric fields, current and density gradient occurring over a period of a few hundred seconds. *Marklund et al.* [2001] showed evidence that the downward current region broadened, as a localized density cavity formed therein. Owing to a finite supply, such broadening was deemed necessary to access more current carriers to sustain a sufficiently large applied current. Using Cluster multipoint measurements and ground based instruments, *Aikio et al.* [2004] showed evidence that density holes that form in the ionosphere adjacent to bright arcs are connected to downward currents and associated with attendant field-aligned current system broadening observed at Cluster altitudes. A sudden expansion of the plasma sheet boundary layer (PSBL) as observed by Cluster during the recovery phase of a substorm is documented by *Aikio et al.* [2008]. Though progress has been made, many aspects of the time development of parallel potential structures have yet to be addressed.

[4] Here we report the results of a detailed case study of the plasma and fields observed by the Cluster spacecraft at key stages of development of a new quasi-static upward and downward auroral arc system of field-aligned currents. The event was observed on February 21, 2001 during a transit of the PSBL at an altitude of ~3 R_E under relatively quiet magnetospheric conditions (Kp = 1^+ and AE~50 nT). This event is of particular interest in that the inverted V arc system formed out of an initial Alfvén wave dominated system of small-scale, field-aligned currents. In past single spacecraft studies these regions were seen as distinct regions.

[5] The multispacecraft measurements presented here indicate that quasistationary arc current systems can be born out of the Alfvén dominated region occurring at the PSBL. This new system appeared to form in response to the local expansion of the plasma sheet via the injection at higher latitude of a new plasma sheet population on previously unoccupied magnetic field lines. The purpose of this study is to assess the properties of the plasma and fields during the transformation process, including the evolution of the current system, the formation of a density cavity and parallel potential drops that occur, and the associated reorganization of the plasma. Within this context, we explore the manner in which changes in the plasma and fields at the high-altitude auroral zone boundary affect the occurrence and size of acceleration potentials in the composite upward and downward current system, and assess consequences of parallel potential development. Though we are presenting a single case example, we believe that the detailed characterization presented here will form a useful basis for comparison with theoretical models and other multispacecraft observations of auroral arc formation processes.

[6] The paper is organized in the following manner. In section 2, we describe the Cluster instrumentation and data sets used. Section 3 is devoted to the detailed presentation of the plasma and field observations that characterize the event. We explore the geometry, motion, and width of the developing density cavity. We provide arguments indicating observed changes are more naturally explained as temporal rather than spatial. Our presentation highlights the evolutionary sequence of the fields and plasma, including detailed distribution function characteristics. Interrelationships between electron temperature and potential are explored. Last, we place the high-altitude Cluster observations in context with global auroral image data from IMAGE. These comparisons show that the high-altitude sequence led to a poleward boundary intensification (PBI). The discussion and conclusions are given in sections 4 and 5.

2. Instrumentation and Experimental Data Set

[7] The primary data set for this study comes from the Cluster spacecraft. Spacecraft potential data used in the timing analysis and for density estimates are provided by the electric field and wave experiment [*Gustafsson et al.*, 1997] at a rate of 5 samples s^{-1}. Ion data are provided by the Cluster Ion Spectrometry (CIS) experiment [*Réme et al.*, 1997]. CIS is composed of two instruments, a Hot Ion Analyzer (HIA) and a time-of-flight ion Composition and Distribution Function Analyzer (CODIF), which measures the major ions in the range 5 eV q^{-1}–40 keV q^{-1}. We will show analyses based on H^+ distribution function data from CODIF and ion data from HIA. Full 3D distributions are sampled every 4–12 s in the auroral zone, depending on mode, and on-board computed moments are sampled at 4 s resolution. We used electron data from the plasma electron and current experiment (PEACE) [*Johnstone et al.*, 1997], which is composed of two sensors mounted on opposite sides of each spacecraft, the Low Energy Electron Analyzer (LEEA) and a High Energy Electron Analyzer (HEEA). Typically, electron fluxes are measured by PEACE-LEEA in the energy range from 0.7 eV to 1 keV, and by PEACE-HEEA from 30 eV to 26 keV. The overlapping data from the two sensors are usually in good agreement, though significant differences do occur and are generally attributable to aliasing in short scale space and/or time variations (LEEA and HEEA sample velocity space half a spin (2 s)

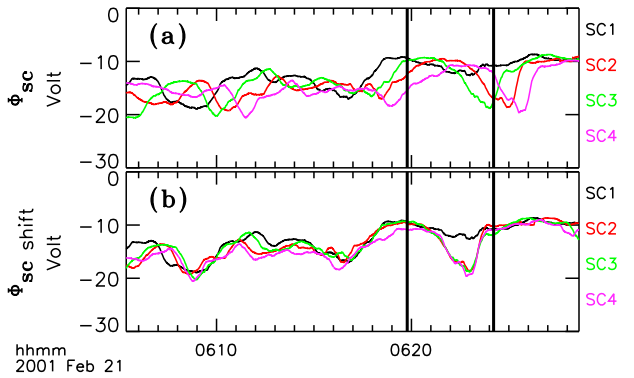

Figure 1. (a) Negative of spacecraft potential profiles for each spacecraft averaged using a 40 s boxcar smoothing window and (b) same potential profiles shifted by time delays relative to SC1 determined from correlation analysis.

out of phase). We also used Fluxgate Magnetometer data [*Balogh et al.*, 1997], for context, to organize particle data, and for estimating currents.

[8] To provide global auroral context, data from the Wideband Imaging Camera (WIC) of the far ultraviolet (FUV) instrument onboard IMAGE is also presented [*Mende et al.*, 2000]. The FUV-WIC instrument is sensitive to the spectral range from 140 to 160 nm and provides images (20 s integration time) every 2 minutes.

3. Observations

3.1. Cavity Geometry, Velocity, and Width

[9] Figure 1a depicts the negative of the spacecraft potential Φ_{SC} (a proxy for density) measured by the four Cluster spacecraft during the auroral zone pass on February 21, 2001. The potential traces have been smoothed using a 40 s sliding average to remove higher frequency structure. The vertical lines delimit a region where a density cavity forms. To get time delays, cross-correlation analysis was applied to all possible pairings of the Φ_{SC} traces in the delimited region. The correlation coefficients are found to have peak values $\geq$0.97 at the determined lag times for the interval, indicating that similar signatures are observed on all 4 SC. The time delays relative to SC1 were found to be dt_{21} = 117 s, dt_{31} = 65 s, and dt_{41} = 164 s, respectively. Figure 1b shows the same Φ_{SC} profiles after shifting to the time line of SC1 by the appropriate delay times. The good alignment of the traces demonstrates that three of the spacecraft observed nearly the same fully developed density cavity near 0623 UT, which had only begun to form when the lead spacecraft SC1 encountered it. Although this example is time dependent, these observations show that the cavity formation is not accompanied by significant expansion transverse to the background magnetic field (based on the cavity normal determined below).

[10] High values for the peak correlation coefficients alone do not establish whether or not the structure is planar and moving at a constant normal velocity, which are required conditions of the timing analysis. A necessary, but not sufficient, condition for planarity and uniform motion is that the cross-correlation lags $dt_{\alpha\beta}$ must be linearly independent. Namely, the relations $dt_{\alpha\beta} + dt_{\beta\gamma} + dt_{\gamma\alpha} = 0$, for all possible spacecraft combinations, must be satisfied to within the expected uncertainties. In this event the residuals of the permuted time delay triplet sums are at or within the expected Nyquist uncertainty of $3\delta t_{\text{Nyquist}} = 1.2$ s, suggesting that the evolving cavity is planar and moving at a constant velocity.

[11] From the given timings [*Harvey*, 1998], we determined a normal to the cavity $\hat{\mathbf{n}}$ = (−0.021, −0.367, −0.930) GSE, which is inclined at an angle $\theta_{Bn} = 80°$ with respect to the magnetic field ($\hat{\mathbf{b}}$ = (0.975, 0.030, −0.220)), and at an angle $\theta_{vn} = 166°$, with respect to the tetrahedron trajectory. Being within ~1° of the magnetic meridional plane, the normal is 10° off the current sheet normal (geomagnetic equatorward direction) defined in a magnetic field aligned coordinate system by the unit vector within the magnetic meridional plane, transverse to the magnetic field. Viewed in light of the existence of fine-scale structure in the magnetic field data the normal is in reasonable agreement (within 17°) of the four normals obtained from minimum variance of the perturbation magnetic field. The cavity velocity relative to Cluster along the normal is $V_{\text{rel}} = 9 \pm 1$ km s^{-1}. This is due in part to the spacecraft velocity along the normal, which is −4.7 km s^{-1}. The remainder is consistent with the convection velocity along the normal estimated at $(\mathbf{E} \times \mathbf{B}/B^2) \cdot \hat{\mathbf{n}} = 7 \pm 2$ km s^{-1} in an Earth fixed frame based on EDI electric field observations adjacent to the cavity. Given the speed, the width of the cavity is estimated to be L_w = (224 s) (9 km s^{-1}) = 2000 ± 200 km ($\approx 200 r_p \approx 130$–$200 \lambda_e$, where r_p is the gyroradius of the plasma sheet proton population, which has an average energy of 4 keV, and λ_e is the electron inertial length, which ranges from 5 km just outside to 17 km within the deepest part of the cavity).

3.2. Arguments for Temporal Evolution

[12] The sequence of events relative to the Cluster spacecraft configuration as the fleet transited the density cavity region suggest that the differences between the Φ_{SC} profiles are temporal rather than spatial. The Cluster spacecraft were in a "cigar-shaped" configuration (elongation E = 0.8 and planarity P = 0.15, defined by *Robert et al.* [1998]), which was preferentially aligned along the normal of the cavity. This is apparent in Figure 2, which shows the spacecraft locations projected onto orthogonal planes con-

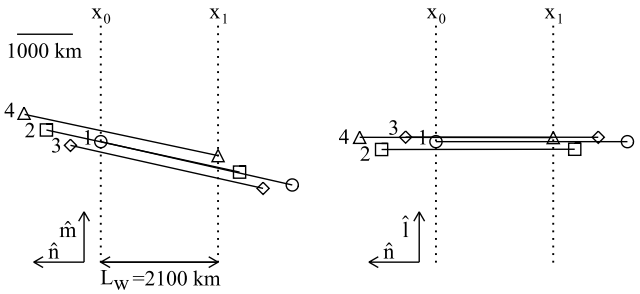

Figure 2. Spacecraft positions projected in the $\hat{\mathbf{n}}$-$\hat{\mathbf{m}}$ and $\hat{\mathbf{n}}$-$\hat{\mathbf{l}}$ planes from the time SC1 encountered the cavity at X_0 until the exit time of SC4 at X_1. SC1 is indicated by circles, SC2 is indicated by squares, SC3 is indicated by diamonds, and SC4 is indicated by triangles. Solid lines connecting the spacecraft symbols indicate the projected orbital paths. The dotted vertical lines delimit the density cavity.

taining the boundary normal. The boundary normal coordinate system is defined using $\hat{\mathbf{l}} \equiv \hat{\mathbf{n}} \times \hat{\mathbf{V}}_{\mathbf{tet}}/|\hat{\mathbf{n}} \times \hat{\mathbf{V}}_{\mathbf{tet}}|$, which is along the magnetic eastward direction, and $\hat{\mathbf{m}} \equiv \hat{\mathbf{n}} \times \hat{\mathbf{l}}$, which is nearly antiparallel to the magnetic field. Here $\hat{\mathbf{V}}_{\mathbf{tet}}$ is the Cluster tetrahedron velocity unit vector. Both the locations at the time when SC1 encountered the cavity and when SC4 exits the cavity are indicated, in addition to the orbital paths. Clearly, the trajectories shown in Figure 2 are not significantly displaced in azimuth ($\hat{\mathbf{l}}$) nor along the magnetic field ($\hat{\mathbf{m}}$). Thus the Cluster fleet makes an invariant latitude transect of the region, at a nearly nearly fixed magnetic local time and altitude along the magnetic field. Also, spatial variations are virtually ruled out because the orbital paths of SC3, SC2 and SC4, which see a deeper cavity, bound that of SC1, which sees a shallow cavity. Further support for the temporal development interpretation is evidenced in additional data from Cluster and from IMAGE presented in section 3.7.

3.3. Evolutionary Sequence of the Plasma and Fields

[13] Figure 3 displays a series of plasma and field measurements from three Cluster spacecraft (SC1, SC3 and SC4) at a poleward crossing of the high-altitude plasma sheet into the polar cap in the northern hemisphere on February 21, 2001 near midnight. For each spacecraft, show the field-aligned (downgoing) and field-opposed (upgoing) proton differential energy flux spectrograms from CODIF, densities, and the east–west perturbation magnetic field are shown. The data from SC3 and SC4 have been shifted to SC1's time line, using the correlation lags given in section 3.1. Vertical lines delimit a region of interest from 0619:50 UT to 0624:10 UT encompassing the plasma sheet-polar cap transition. The data sets are displayed in the order, from top to bottom, in which each spacecraft encountered the region, with SC1 encountering it first, followed by SC3 65 s later, and SC4 164 s later. Though the analysis was applied to spacecraft potential data, it is clear that the correlation results organize the other properties of the developing arc system and signifies that the cavity is an inherent part of the arc system as a whole. Below we describe the time sequence of events.

[14] With He^+ and O^+ constituting only a few percent of the ions in the delimited region, we focus on the dominant H^+. The plasma sheet H^+ are well sampled in the CIS-CODIF energy range and appear, at this altitude, with nearly symmetric field-aligned and field-opposed differential energy fluxes above 1 keV. Noteworthy is the apparent 0.3–0.4° invariant latitude displacement of the ion plasma sheet boundary observed by SC3 and SC4 relative to that encountered by SC1. For SC1 (Figures 3a and 3b), the plasma sheet H^+ extends out to ~0622:20 UT before becoming significantly diffuse in transition to the polar cap. By the time SC3 crosses nearly the same location ~1 minute later (Figures 3e and 3f) we see the same boundary, and then poleward a new, more intense population of energy latitude dispersed plasma sheet H^+ [e.g., *Bosqued*, 1987; *Zelenyi et al.*, 1990] from ~0622:20–0625:00 UT. This new population is still present during SC4's passage of the region nearly three minutes later (Figures 3i and 3j). Thus according to SC3 and SC4, the ion plasma sheet is thicker than when seen by SC1. This extension of the plasma sheet to higher latitudes cannot be explained as tail flapping or large-scale surface waves because this region is moving equatorward at the convection velocity. These results suggest that the plasma sheet is thicker by virtue of the injection of a new hot plasma sheet population onto higher latitude field lines, creating a poleward displacement of the last closed field line.

[15] Coincident with the newly injected plasma sheet ions is the occurrence of upgoing ions at ~0622–0623 UT (Figures 3f and 3j) in a region associated with a large scale upward field-aligned current, inferred from the positive slope in the perturbation magnetic field (Figures 3h and 3l). These ions indicate a parallel potential has formed below SC3 and SC4. Transverse ion heating at lower altitudes coupled with adiabatic invariance constraining ion motion up the field line can lead to similar signatures. However, we can rule this possibility out since coincident electrons discussed below show distribution signatures in favor of the potential formation interpretation. No significant signatures of energetic upflowing ions were recorded by SC1 in this interval (Figure 3b).

[16] In addition, a density cavity forms in the region encompassing the newly injected plasma sheet ions and the ion outflow. Densities estimated from electron (red curve), proton (blue) and high time resolution spacecraft potential (black) measurements are shown in Figures 3c, 3g, and 3k. These have been intercalibrated using density data (not shown) from WHISPER [*Décréau et al.*, 1997] over the current epoch. Gaps in N_{SC}, the density estimate from Φ_{SC}, are brief intervals during which the spacecraft potential measurements were perturbed by the WHISPER sounder experiment. Cavity formation is most apparent in the spacecraft potential and electron density estimates. According to SC1 data, the cavity is, in large part, quite shallow, whereas SC3 and SC4 see a deep cavity. Also, the cavity is ultimately deeper in a localized downward current region which forms during 0622:50–0623:30 UT (Figure 3k). According to the high time resolution spacecraft potential estimates, the density outside the cavity, N_{out}, seen by SC1 is ~1.2 cm^{-3} and the interior density, N_{in}, is typically ~0.8 cm^{-3}, though it reaches a minimum value of 0.3 cm^{-3} in the downward current region near ~0623:00 UT. These values yield a typical density ratio of $N_{out}/N_{in} \sim 1.5$, with a peak value of ~4.0 in the localized downward current region. By the time SC3 and SC4 encountered the cavity, the density had eroded significantly. The shape of the cavity is asymmetric, with the density being much lower in the downward current region. The density ratio observed by SC3 and SC4 in upward current part of the cavity is fixed at a constant value of ~4, while peak ratios of ~8 and ~12 for SC3 and SC4, respectively, occur in the downward current part.

[17] The departure of the H^+ density profile from the electron and spacecraft potential counterparts allows us to infer important changes in the ion populations during cavity formation. Initially, the H^+ density shows an order of magnitude departure from the electron and spacecraft potential density estimates within the shallow cavity and into the polar cap region. These indicate that a sizable fraction of the ion population has energies $\lesssim$30 eV. These ions are not registered by CODIF, due to repulsion of ions by the $\gtrsim$10 eV spacecraft potential in the vicinity of the cavity and the 20 eV low-energy threshold of this detector. This low energy ion population dominates the density within the cavity, especially

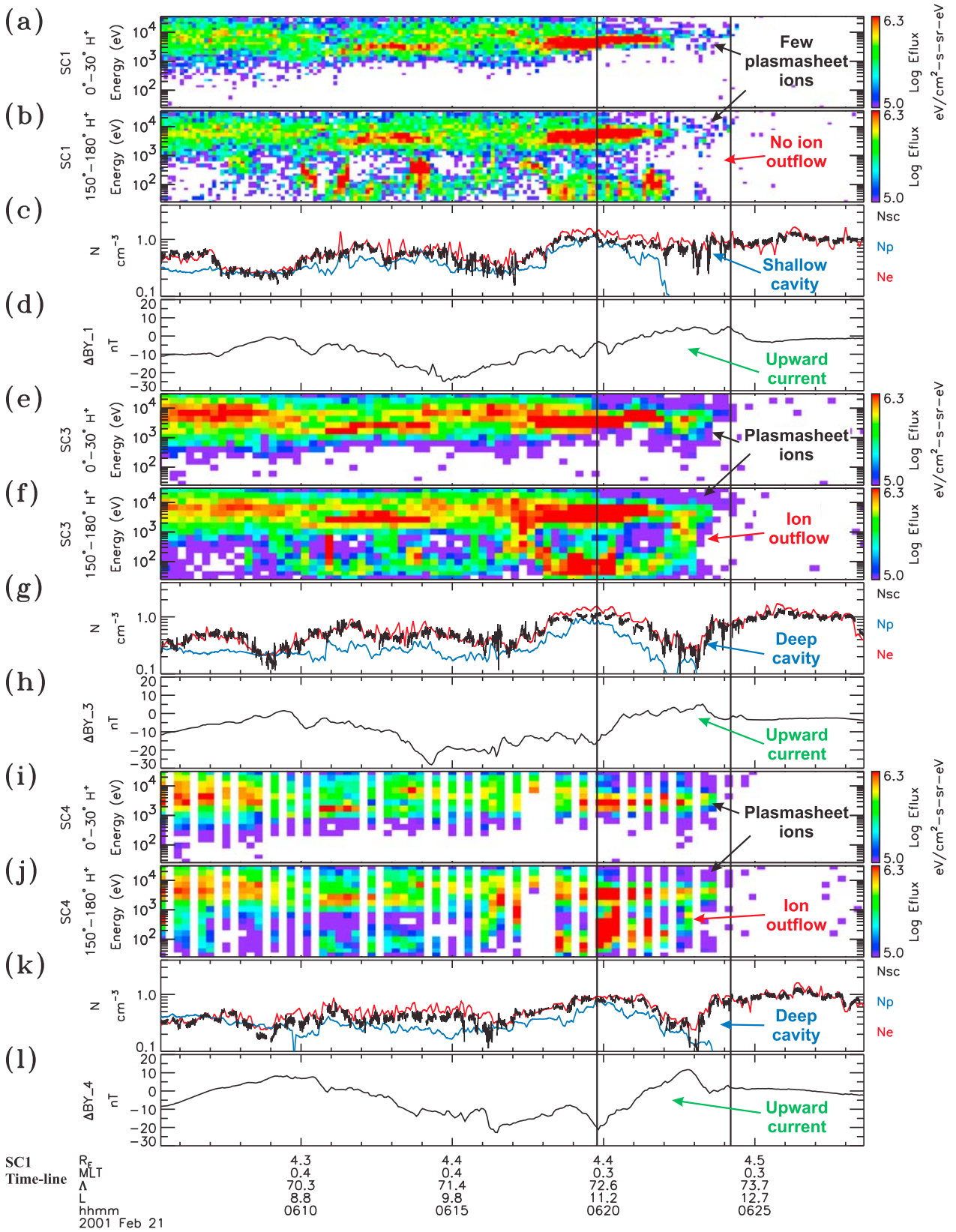

Figure 3. Shows spectrograms of (a, e, and i) field-aligned and (b, f, and j) field-opposed H^+ differential energy flux; (c, g, and k) densities estimated from electron (red), proton (blue), and spacecraft potential (black) measurements; and (d, h, and l) the east–west perturbation magnetic field as observed from three of the Cluster spacecraft: SC1 (Figures 3a–3d), SC3 (Figures 3e–3h), and SC4 (Figures 3i–3l). The data from SC3 and SC4 have been shifted to SC1's time line, using the correlation lags.

in the latter half of the delimited interval in Figure 3c and also in the polar cap. By the time SC3 and SC4 encounter the cavity, the different estimates of density are in better agreement (within a factor of two), particularly in the upward current region where the ions consist of energetic injected plasma sheet protons and outflowing protons that have been accelerated into the CODIF's range by the parallel electric field. These results allow us to infer that the cold, relatively dense, low-energy ion population, initially occurring in the cavity region, has been replaced by tenuous energetic plasma sheet ions and ion outflow during the formation of the arc system.

[18] The current also undergoes significant changes during Cluster's transit time. In the interval of interest the perturbation magnetic field ΔBY seen by SC1 and SC3 is highly irregular due to the presence of small-scale structure superposed on top of large scale variations (see Figures 3d and 3h). Note that increases in ΔBY with respect to time indicate regions of magnetic field-aligned (upward) current and decreases indicate regions of antialigned (downward) current. These small-scale structures have durations approximately less than a few tens of seconds, with magnetic field deflections ranging from a few nT to ~10 nT in SC1 (Figure 3d), SC2 (not shown), and SC3 (Figure 3h) data. The ratio of $E_{\perp n,l}/B_{\perp l,n}$ associated with the substructure in the cavity is estimated to be on the order of the local Alfvén speed (10,000–16,000 km/s in the cavity) suggesting that these are Alfvén waves. Although the current encountered by SC1 is highly irregular, a large-scale current pattern is discernible. The interval from 0610–615 UT is characterized by a large-scale, downward current, while 0615–0624 UT exhibits a large-scale, upward current that extends into the cavity region. On SC3, signs of a forming large-scale, up-down current sheet pair begin to appear with superposed fine structure in the cavity region. It is interesting to note that the large-scale, upward current region maintains its slope in the interval from 0620:30–0623:20 UT, but for the interval 40s prior to this shows an intensified current. This suggests that the initial development of the parallel potential drop within the upward current part of the cavity is due to some controlling factor other than a changing large-scale current (see discussion below). On SC4, we see that the up-down current sheet pair has strengthened as the fine structure has attenuated (Figure 3l). The current sheet pair is asymmetric, with the overall transverse width of the upward current part spanning 1620 km and the downward component extending 340 km. This asymmetry is coincident with and probably connected to the asymmetric depletion of the density (Figure 3k). A detailed description of the currents within the cavity is given below in section 3.4.

[19] Figure 4 depicts electron data observed by PEACE during the same time interval. These data also have been shifted to SC1's time line and are presented in the order each spacecraft encountered the cavity (SC1, SC3, SC2 and then SC4). For each spacecraft it shows differential energy flux spectrograms versus energy and pitch angle, and the east–west perturbation magnetic field. The white curve in the spectrograms indicates the spacecraft potential. The same region of interest where the cavity forms is delimited by the solid vertical lines. Note that the faint fluxes seen in the polar cap after 0625 UT, which are peaked near 90° in the pitch angle spectrograms, are an instrumental artifact. This weak noise primarily occurs in the lower energy channels, and does not significantly affect the electron signatures presented below.

[20] As with the protons, the electron spectrograms show that the plasma sheet had expanded by the time SC4 entered the cavity. The sequence of events here confirms the picture of the expansion being due to the injection of new plasma as opposed to a poleward motion of the plasma sheet. According to SC1 (Figure 4a), the plasma sheet electrons occur at energies from ~0.5–4 keV in the interval from 0605 UT to ~0622 UT, which extends over part of the delimited region. In addition to this population, low-energy ($\lesssim$400 eV) electrons occur intermittently throughout the interval. Well within the plasma sheet (from ~0605–0620 UT) these low-energy electrons, which are associated with small-scale downward currents, appear as either upgoing (180° pitch angle) or counterstreaming enhancements in the pitch angle spectrograms for 30–400 eV electrons. Within the delimited region, the lower-energy electrons are preferentially aligned parallel and antiparallel to the magnetic field, but span a much broader energy and pitch angle range than in the earlier interval. These electrons, associated with small-scale currents, are similar to those observed at low altitudes in the plasma sheet boundary layer. This region has been denoted as the Alfvén region, so as to be distinguished from relatively more stable adjacent upward and downward current regions occurring well within the plasma sheet [see *Paschmann et al.*, 2003, chapter 4, and references therein].

[21] Nearly a minute later, a new, hot plasma sheet electron population in the energy range from ~0.5–4 keV is observed by SC3 during 0622:20–0623:00 UT, poleward of the preexisting electron plasma sheet boundary (Figure 4d). This new population is coincident with the occurrence of the injected plasma sheet ions and upgoing ions observed by SC3 (Figures 3e and 3f). In addition fine-structured, Alfvén wave modulated, low-energy electrons are still prominent in the region. By the time SC2 and SC4 traversed the cavity region 2 minutes and 2.7 minutes after SC1, the new plasma sheet electron population expanded equatorward, with its equatorward edge eventually merging with the preexisting boundary at ~0622 UT (Figures 4g and 4j). Moreover, the fine structuring in the low-energy electrons diminished as an up-down current system, acceleration potentials and the density cavity formed. As will be shown in more detail below, the plasma sheet electrons in the upward current part of the cavity are characterized by a loss cone distribution with suppressed fluxes in the field-opposed direction, with dropouts at low energy (as indicated in Figures 4j and 4k). In the adjacent downward current region from 0622:55 UT to 0623:35 UT, the plasma sheet populations are characterized by diminished energy flux levels, and are accompanied by upgoing and/or counterstreaming electrons. This time sequence, along with the evolution of the currents described earlier, shows that the dynamically varying Alfvén region has evolved into a more clearly defined, and quasi-stationary up-down current system, with inverted V auroral arc signatures. As we will discuss below, this observed sequence suggests that the dynamic Alfvén region encompassed by the cavity may have been stabilized by the injection process.

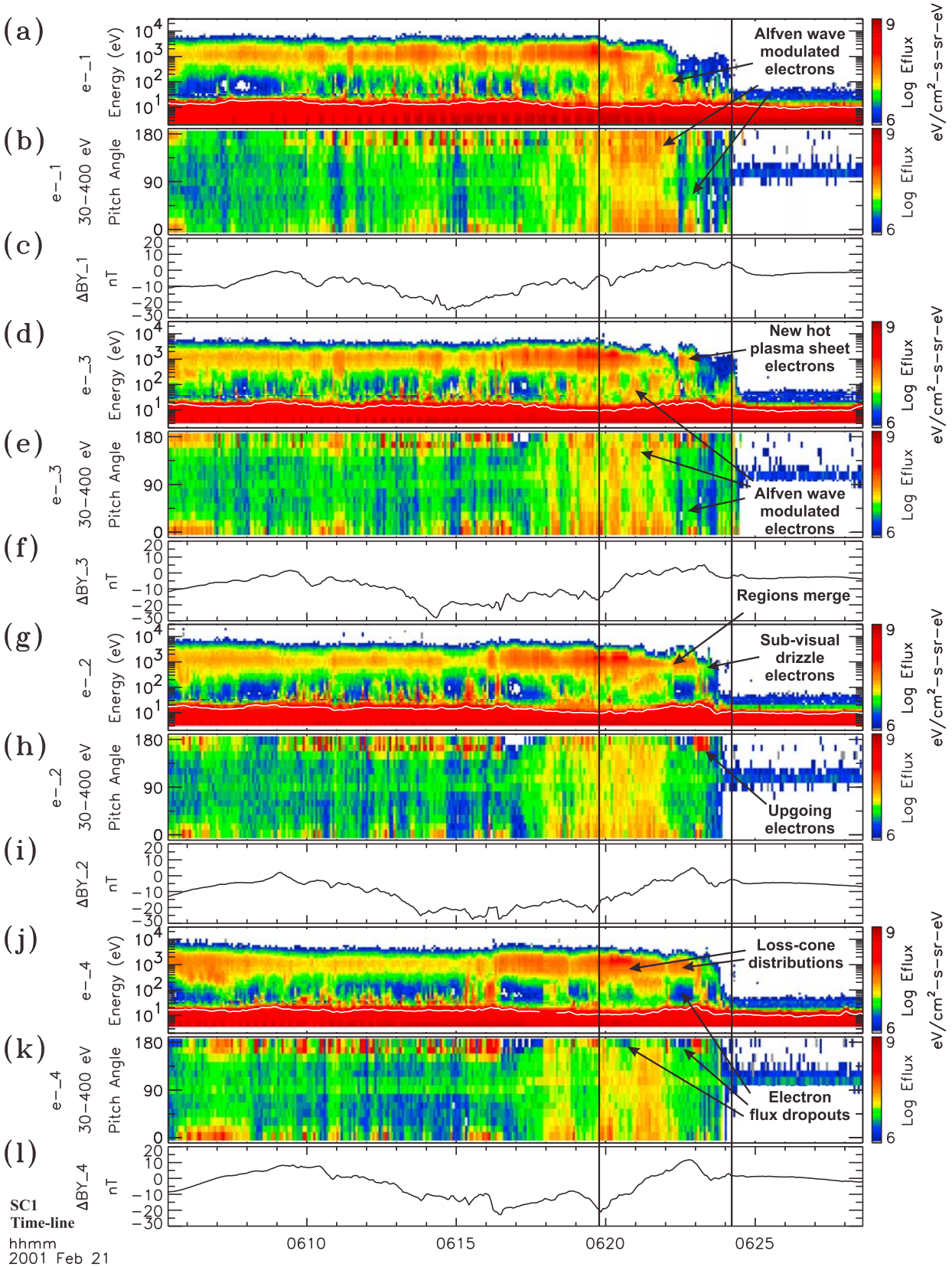

Figure 4. Spectrograms of electron differential energy flux versus (a, d, g, and j) energy and (b, e, h, and k) pitch angle, and (c, f, i, and l) perturbation magnetic field observed by SC1 (Figures 4a–4c), SC3 (Figures 4d–4f), SC2 (Figures 4g–4i), and SC4 (Figures 4j–4l). Solid vertical lines indicate the cavity region. The white curve in Figures 4a, 4c, 4e, and 4g indicates the spacecraft potential. The data from SC2–SC4 have been shifted to SC1's time line, using the correlation lags.

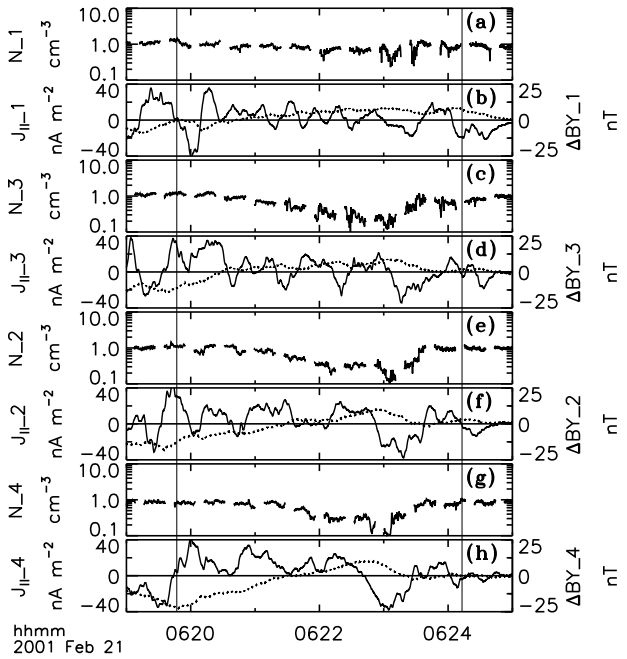

Figure 5. Spacecraft (a, c, e, and g) potential estimates of densities and (b, d, f, and h) parallel current densities estimated from ΔBY in the cavity region for each spacecraft: SC1 (Figures 5a and 5b), SC3 (Figures 5c and 5d), SC2 (Figures 5e and 5f), and SC4 (Figures 5g and 5h). For context, ΔBY (dotted curve) is included in Figures 5b, 5d, 5f, and 5h. The data from SC2–SC4 have been shifted to SC1's time line.

3.4. Evolution of Current Within the Cavity

[22] The temporal changes in the current within the cavity are made apparent in Figures 5b, 5d, 5f, and 5h, which show parallel current densities for SC1, SC3, SC2 and SC4 focused over the region of interest. Positive values correspond to upward (field opposed) currents and negative values correspond to downward (field aligned) currents. These profiles are shown in the time sequence at which each spacecraft traversed the region. Current densities were estimated from ΔBY measurements assuming that all of the structures of interest are sheet-like spatial structures that convect with the cavity. The current sheet assumption is motivated by the timing analysis presented above and variance analysis applied to ΔB, which yielded well separated eigenvalues for both large-scale and individual small-scale structures, a necessary but not sufficient condition for a sheet approximation. Densities for each spacecraft are provided as a reference (Figures 5a, 5c, 5e, and 5g). Consistent with the "Alfvén region" paradigm, Figure 5b shows that large-amplitude, small-scale Alfvénic fluctuations initially dominate the current in the cavity region. The large-amplitude fluctuations are well-correlated with the fine structure in the electrons and upgoing ions (discussed above in section 3.3). These fluctuations have amplitudes reaching $J_{\|} \sim 40$ nA m^{-2}, which maps to a value of 3.5 μA m^{-2} at ionospheric altitude, assuming a dipole magnetic field model and $J_{\|}/B$ is constant. For comparison, the initial background (large scale) upward current density in the cavity is ~3 nA m^{-2}, which maps to an ionospheric value of ~0.26 μA m^{-2}. Based on power spectral density (PSD) comparisons shown below, the small-scale currents are characterized by transverse widths ranging from 30 km to 225 km, with the larger amplitude signatures typically corresponding to ~80 km widths. (Note widths correspond to half transverse wavelengths $\lambda_{\perp}/2$.) At ionospheric altitudes these values lead to widths ranging from 3 to 20 km. In subsequent passages by the other spacecraft it is clear that the amplitudes of the small-scale currents attenuate as the region transitions to a larger scale up-down current sheet pair. On SC4, the upward current part of the cavity (from ~0619:50–0622:50 in Figure 5h) is associated with large-scale, positive definite variations in the current density peaking at ~40 nA m^{-2}, with an average (background) value of ~14 nA m^{-2}. These map to ionospheric values of 3.5 μA m^{-2} and 1.2 μA m^{-2}, respectively. These larger-scale variations are associated with variations in quasi-static inverted V electron signatures observed by SC4 discussed above (see Figures 4j and 4k). The downward current density attains a peak absolute value of ~40 nA m^{-2}, which corresponds to an ionospheric value of 3.5 μA m^{-2}. The overall widths of the large-scale upward and downward current sheets reported above map to thicknesses of 173 km and 38 km, respectively, at ionospheric altitudes, which are much larger than the typical widths (~8 km) of the small-scale Alfvénic currents seen in Figure 5.

[23] The small-scale Alfvénic currents attenuated as their transverse wavelengths approached the electron inertial scale. This suggests that inertial effects may have played a role, whereby the structures become dispersive and thus susceptible to damping. The frequency regime associated with the attenuation is made apparent in comparisons of power spectral density (PSD) of the transverse perturbation magnetic field ΔB in the cavity for SC1 and SC4 as a function of frequency shown in Figure 6a and the ratio

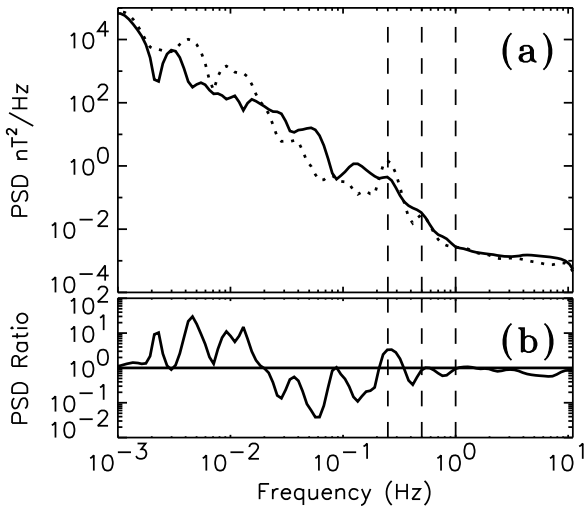

Figure 6. (a) Power spectral density (PSD) of ΔB as a function of frequency for SC1 (solid curve) and SC4 (dotted curve) and (b) the ratio between SC4 ΔB PSD and SC1 PSD as function of frequency. PSDs were computed via a Morlet wavelet transform. The spurious spin tone signature and harmonics are indicated by dashed vertical lines.

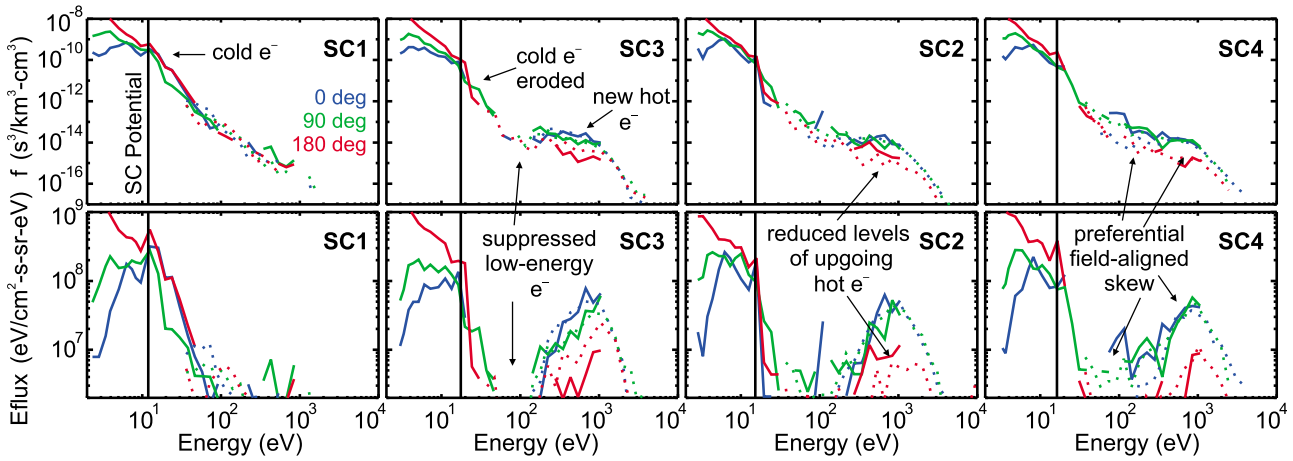

Figure 7. (top) Time sequence of electron phase space densities observed in nearly the same upward current part of the cavity encountered by SC1, SC3, SC2, and SC4 (~0622:35 UT in Figure 4) and (bottom) time sequence of differential energy fluxes. Times for SC3, SC2, and SC4 have been corrected for time delay. Blue indicates precipitating electrons, red indicates outflowing electrons, and green indicates electrons perpendicular to the magnetic field. Data from LEEA are indicated by the solid curves and HEEA by the dotted curves. The solid vertical line indicates the measured spacecraft potential.

between the SC4 and SC1 ΔB PSDs shown in Figure 6b. The SC4 PSD is enhanced (up to a factor of 30) relative to that from SC1 at frequencies from 2 mHz to 20 mHz, in association with the growth of the large-scale current. Fluctuations are attenuated at frequencies between ~25 mHz and ~150 mHz, with a peak drop in PSD (factor of 30) near 60 mHz corresponding to the large-amplitude, small-scale currents seen in Figure 5b. Spurious spin tone and harmonics in the spectra (dashed vertical lines) and intensities approaching FGMs sensitivity floor make comparisons ambiguous at frequencies above ~150 mHz. Assuming that they are spatial structures that convect with the cavity, these frequencies correspond to transverse wavelengths $\lambda_\perp$ ranging from 60 km to 450 km. Inertial effects become important when the ratio $\epsilon = 2\pi\lambda_e/\lambda_\perp \sim 1$. During SC1's traversal of the region, $\epsilon \sim 0.07$–0.5 (for $\lambda_e \approx 5 \pm 2$ km) in the cavity region, which are primarily below the criteria. During SC4's traversal of the region, the λ_e increased and we find that $\varepsilon \geq 0.5$ for frequencies $f = 0.5V_{\rm rel}/2\pi\lambda_e \geq 70 \pm 30$ mHz ($\lambda_e \approx 10 \pm 3$ km) and $f \geq 50 \pm 20$ mHz ($\lambda_e \approx 15 \pm 9$ km) in the upward and downward current regions of the cavity, respectively. With much of the attenuated frequencies falling within the criteria, inertial effects can not be ruled out, with consequential damping at and/or above Cluster's altitude providing a plausible explanation for the attenuation of small-scale Alfvénic fluctuations.

3.5. Distribution Functions Within the Cavity

[24] In addition to providing key insight into the nature of the developing potential, the electron and ion distribution functions reveal the detailed reorganization of plasma constituents that take place as the arc system develops. Here we show that the formation of the density cavity described above is primarily an artifact of an erosion of cold dense electrons and acceleration of ions in the upward current region, and vice versa in the downward current region. This density depletion coincides with the injection of a hot tenuous magnetospheric source electron component, that seems to control the development of a parallel potential in both the upward and downward current region.

3.5.1. Upward Current Region

[25] The time sequence (left to right) of electron distributions in the upward current part of the developing density cavity is shown in Figure 7. Based on correlation delay times, these data were sampled from nearly the same location in the cavity, where the energetic upgoing ions were observed to occur (at 0622:34 UT in Figure 3). Figure 7 (top) shows electron phase space densities for SC1, SC3, SC2 and SC4, while Figure 7 (bottom) shows differential energy fluxes. The spectra are color coded to indicate magnetic field-aligned (blue), field-opposed (red), and perpendicular (green) pitch angles, respectively. The plots show data from both LEEA (solid curve) and HEEA (dotted curve), which overlap in the energy range from 30 eV to 1keV. The solid vertical lines indicate the measured spacecraft potentials. Ambient electrons, which have been shifted up in energy by the positive spacecraft potential, determine the spectra to the right of this line; spacecraft generated photoelectrons determine the spectra to the left of this line.

[26] The ambient electrons observed by SC1 are characterized by a power law distribution function which extends from the spacecraft potential to a few hundred eV. This population is relatively cold ($T_{e1} \sim 15$ eV) and dominates the density (~0.8 cm^{-3}) in the cavity. During this interval there are no precipitating $\gtrsim$1 keV electrons within or poleward of the cavity. Therefore we do not expect significant contributions to the low-energy component from backscattered secondaries.

[27] By the time SC3 encountered the region 64 s later, there was a significant reduction in this cold electron population, as evident from the order of magnitude reduction of the peak phase space density and significant drop out in the

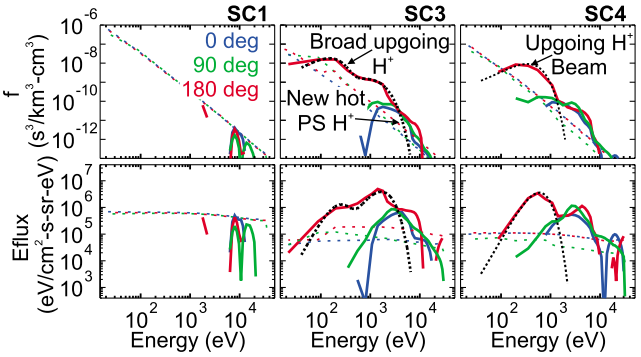

Figure 8. (top) Time sequence of proton phase space densities observed by CODIF in nearly the same upward current part of the cavity (~0622:35 UT in Figure 4) encountered by SC1, SC3, and SC4 and (bottom) time sequence of differential energy fluxes. Times for SC3 and SC4 have been corrected for time delay. Blue indicates precipitating protons, red indicates outflowing protons, and green indicates protons perpendicular to the magnetic field. The black dotted trace indicates fits to upgoing proton distributions. The dashed line indicates the one count level.

electron energy flux below 100 eV relative to SC1 data (Figure 7). In addition, there now exists an energetic electron component at energies from 100 eV up to ~2 keV. This new population has a density of ~0.2 cm^{-3} and temperature of ~613 eV. Figure 7 shows that similar distribution functions were observed by SC2 and SC4, with respective temperatures of 830 eV and 560 eV and densities of 0.3 cm^{-3}.

[28] The distributions observed by SC3, SC2, and SC4 at these high altitudes have features consistent with a loss cone distribution modified by the presence of a parallel potential drop below the spacecraft due to an upward directed parallel electric field [e.g., *Kletzing and Scudder*, 1999]. Although PEACE is not able to fully resolve the loss cone, estimated to be ~7° at this altitude, the existence of such a feature is indicated by the preferential field aligned (downgoing) skew at energies above a few 100 eV. Reduced fluxes at low energy are a persistent feature in SC3, SC2, and SC4 data in Figure 4 found to be coincident with upgoing energetic ions (shown in Figure 3 and discussed below) in regions of upward current. An upward directed parallel electric field would prevent ionospheric photoelectrons, backscattered electrons and atmospheric secondaries from reaching this high altitude.

[29] Figure 8 shows proton distributions for SC1, SC3, and SC4 within the upward current part of the cavity in the time order each spacecraft crossed the region. These proton data were sampled from nearly the same location as the electron data shown in Figure 7 and are shown using a similar format. Here, we only discuss the features of the proton distributions, since they are the dominant constituent in the region. The proton samples from SC3 and SC4 are coarsely sampled (with a 12 s integration time), yielding only a few distributions in the region. We do not address the evolution of the cold proton kinetic properties. This component is not sampled by CODIF, because they get reflected by the spacecraft's positive potential. The evolution of these ions has been inferred, in part, by electron-ion density differences described above. Nevertheless, the parts of the distribution that are measured do have distinct features indicative of the expansion of the plasma sheet and consequent development of a parallel potential drop below the spacecraft.

[30] Initially, SC1 sees few plasma sheet protons (Figure 8). No evidence of upgoing protons is seen. When SC3 encountered the region, we see a new hot plasma sheet proton population occur at energies from 1keV to 10 keV (SC3 in Figure 8). Also, field-opposed (upgoing) protons are observed to occur over a broad energy range extending from ~50 eV up to ~3 keV before becoming less distinguished from the new plasma sheet constituent. A reasonable interpretation of the broad spectrum is that it reflects aliasing of subsequently sampled beams with different energies during the three-spin integration time. This could be due to spatial and/or temporal variation of the potential below the spacecraft. We found a good overall fit to the spectrum below 5 keV using two Maxwellians (black dotted curve) with peak energies of 140 eV and 700 eV and temperatures of 30 eV and 300 eV, respectively. Subsequent passage by SC4 (Figure 8) indicates that the hot energetic plasma sheet population persists and that the upgoing proton spectrum only has a single peak at 340 eV and has a temperature of 70 eV.

[31] The upgoing protons observed by SC3 and SC4 within the upward current region indicate that a parallel potential had developed below these spacecraft, consistent with inferences made from coincident electron distributions discussed above. A reasonable estimate of the potential drop is obtainable from the characteristic energy of the upgoing protons, defined here as the energy flux divided by the number flux [e.g., *Reiff et al.*, 1988; *McFadden et al.*, 1999]. The characteristic energy of upgoing protons seen by SC3 computed using the whole distribution was ~930 eV, with the individual Maxwellian fits having characteristic energies of 210 eV and 1400 eV, respectively. The singly peaked proton beam subsequently observed by SC4 had a characteristic energy of ~630 eV, and suggests that by this time the potential was uniformly distributed over a larger spatial extent and/or had stabilized in time. Whether we adopt the full upgoing distribution value of ~930 eV or the maximum value of 1400 eV for SC3, the reduction to ~630 eV by the time SC4 observed the ions indicates a relaxation of the potential following a peak. We develop further the interpretation of these ion observations in context of other measurements in section 4.

3.5.2. Downward Current Region

[32] Figure 9 shows the electron distribution time sequence observed at nearly the same location within the downward current part of the cavity (~0623:03 UT in Figure 4). Initially, SC1 data indicates the presence of cold (~10 eV), low-energy electrons with a preferential upward skew. This component persisted during SC3's passage of the region, but was depleted by the time SC2 and SC4 encountered the region.

[33] The depletion of cold electrons coincided with the injection of a new, relatively hot plasma sheet electron population. These electrons are observed to occur in the downward current part of the cavity and are associated with peak differential energy fluxes (~2 × 10^7 eV/cm^2 s sr eV) that are reduced relative to the adjacent upward current region value by factors of 2 to 4 depending on spacecraft. *Newell et al.* [1996] noted the presence of a similar electron

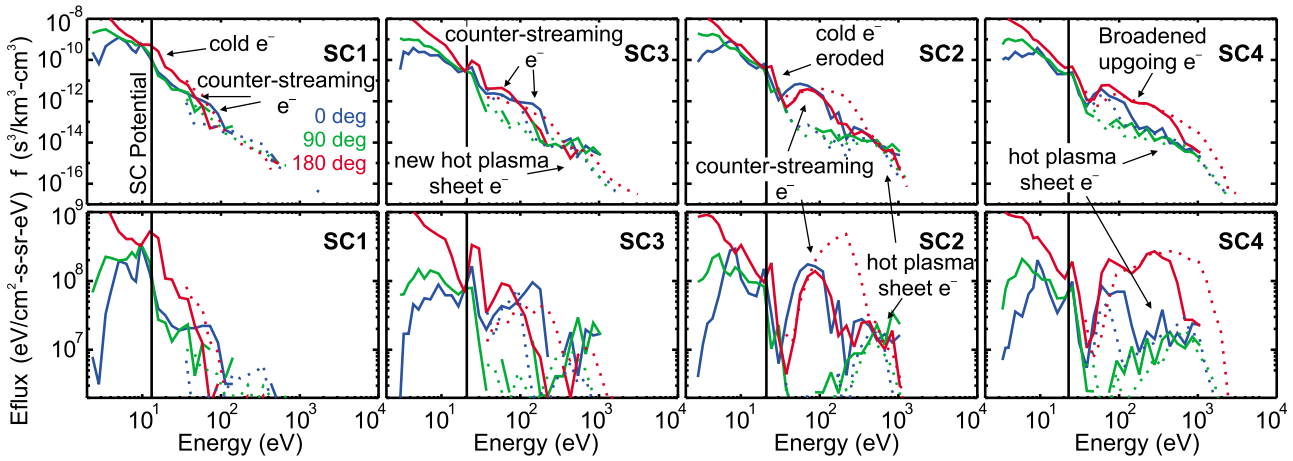

Figure 9. Time sequence of (top) electron phase space density and (bottom) energy flux observed in nearly the same downward current part of the cavity (~0623:03 UT in Figure 4) shown in the same format as Figure 7.

population they denoted "subvisual drizzle" at the poleward edge of the plasma sheet boundary layer, which were physically distinct from polar rain seen at higher latitudes. We can see here that this population may be associated with regions of downward current (as is the case in Figure 4g). Initially, this new population shows up as a distinct shoulder at energies above ~100 eV. In subsequent passes by the other three spacecraft, this shoulder extends to higher energies, resulting in distribution functions that are plateaued or have a gradual negative slope at low energy and drop off sharply at higher energy (above ~600 eV to 1 keV depending on spacecraft), similar to that seen in the adjacent upward current region. However, unlike the upward current counterpart, the distribution spectra associated with this hot plasma sheet component are not suppressed antiparallel to the magnetic field (red curve), and therefore do not show a preferential downgoing skew. This latter feature is discernible in the distribution function (energy flux) spectra above ~300 eV from SC3 and SC2 shown in Figure 9. The differences in the plasma sheet distribution spectra observed within the upward and downward current regions are reflective of the sense of the parallel electric field occurring within these regions. The downward directed parallel electric field in the downward current acceleration region facilitates ionospheric electron access to this altitude, whereas the parallel electric field in the upward current region accelerates downgoing magnetospheric plasma sheet electrons and inhibits ionospheric electrons from accessing this altitude. Though lower relative to upward current values, the plasma sheet electron temperatures are increasing in time, with values estimated at 173 eV, 334 eV, and 430 eV from SC3, SC2 and SC4 measurements, respectively.

[34] Figure 9 shows that counterstreaming electrons are observed to occur in concert with the injection of the hot plasma sheet electrons and the depletion of cold electrons. In SC1 data the counterstreaming electrons appear as the magnetic field-aligned and field-opposed populations at low energy. These populations extended to higher energy during SC3's transit of the region, and were seen as distinct counterstreaming beams during subsequent transits by SC2 and SC4. The counterstreaming electrons are narrow in pitch angle. We estimated the potential drop below the spacecraft using upgoing electron characteristic energies from PEACE LEEA, after correcting for spacecraft potential. These values are ~10 eV, ~40 eV, 50 eV, and ~100 eV from SC1, SC3, SC2, and SC4, respectively. These indicate an order of magnitude growth in the downward current region potential over the span of a few minutes, which coincided with an increase in the source plasma sheet electron temperature (and density).

[35] The interleaved LEEA (solid) and HEEA (dotted) samples of the electron distributions shown in Figure 9 do show differences in the peak energy and temperatures of the counterstreaming beams, which may indicate short scale temporal (2s) and/or spatial (≤20 km) variations. Comparisons (not shown) with adjacent spin period LEEA (solid) and HEEA (dotted) upgoing distribution samples, particularly from SC2 and SC4, reveal that the peak energies are not modulated, but show variations consistent with the in-out traversal of the spacecraft above a U-shaped downward current potential. Thus, we interpret the observed differences in the LEEA (solid) and HEEA (dotted) upgoing electron distributions to be primarily a spatial effect, rather than temporal. We note that by the time SC4 observed the downward current region the upgoing electron beam was substantially broadened in energy, while retaining a narrow pitch angle range. This is consistent with lower-altitude observations and simulations, which attributed such distributions to upward acceleration through a thin potential layer followed by parallel heating via wave-particle processes [e.g., *Ergun et al.*, 2001; *Andersson et al.*, 2002; *Newman et al.*, 2001].

[36] CIS observed no conics in the downward current region 0622:50–0623:30 UT, although we note that SC4 did not sample in the cavity minimum. This may indicate that there was too little transverse heating for the ions to overcome the potential with the aid of the mirror force. Alternatively, sufficient heating did occur, but they did not have enough time to reach this altitude.

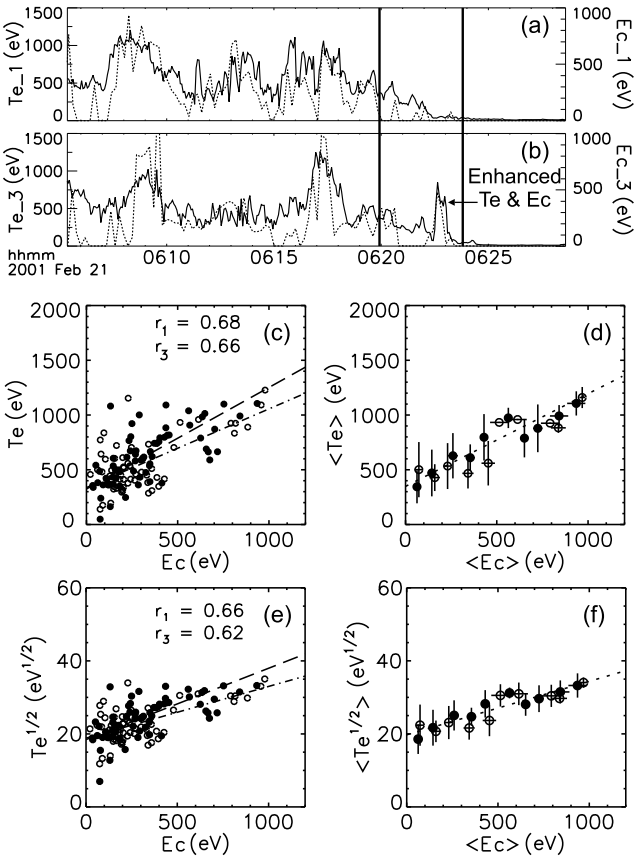

Figure 10. Profiles of the electron temperature (solid) and ion characteristic energy (dotted) determined from CIS-HIA ion spectra from (a) SC1 and (b) SC3. Vertical lines delimit the cavity region. (c) Electron temperature as a function of the ion characteristic energy for SC1 (solid circles) and SC3 (open circles), (d) bin average electron temperature versus average ion characteristic energy. (e and f) Same as Figures 10c and 10d but with square root of electron temperature.

3.6. Temperature Control of Potential Development

[37] The well-known Knight relation [*Knight*, 1973] indicates that the parallel potential drop in a time stationary auroral acceleration region depends on the magnetospheric source electron density and temperature, and the current density. The degree to which the Knight relation is satisfied in this time evolving system is not clear, nor is it the intent here to demonstrate the validity of such a relation. The multipoint measurements do allow us to explore how changes in parameters such as the source electron density and temperature affect changes in the potential. We have noted that the large-scale upward current within the cavity intensified only after SC3 had seen evidence of a field-aligned potential forming. The large-scale current densities for SC1 and SC3 remained constant at ~3 nA m^{-2}. The key point here is that the initial development of the potential did not appear to be driven by a change in the large-scale current. Under these constant current conditions, heuristic arguments based on the Knight relation suggest that the potential should increase as the source density decreases. However, we showed that the drop in density was due to the combined effect of an erosion of a cold dense ionospheric plasma together with an increase in the magnetospheric source plasma density. Such an increase if the Knight relation were to be valid should restrict the size of the potential. Comparisons within the cavity and adjacent region do show a strong correspondence between electron temperature and the potential.

[38] Figures 10a and 10b show electron temperatures (solid) and ion characteristic energies (dotted) for SC1 and SC3, respectively. The temperatures were estimated from merged PEACE LEEA and HEEA data. The ion characteristic energies are computed by dividing CIS-HIA ion energy fluxes by number fluxes. We note that in this event ion characteristic energy enhancements are observed to occur primarily in localized upward current regions, where they serve as a good proxy for the potential drop below the spacecraft. In Figures 10a and 10b a correlation, both within the delimited cavity region and elsewhere, is readily apparent from these time series plots. Notice the increase in ion characteristic energy seen by SC3, over that seen by SC1, as it traversed the upward current part of the cavity from 0622:20–0623:00 UT. This was accompanied by a sharp electron temperature increase, which was due to the newly injected, hot magnetospheric population. This suggests that the electron temperature is an important, if not dominant, factor in determining the occurrence and amplitude of the parallel potential there. Moreover, the correlation seen over the entire 0605–0625 UT interval suggests a more general temperature control of upward current region parallel potential.

[39] Figure 10c quantifies the relationship between electron temperature and ion characteristic energy E_c from SC1 and SC3, respectively, for the full interval shown in Figure 10a. Here the more frequent electron temperatures were boxcar averaged to the ion sampling resolution. The linear correlation coefficients are 0.68 and 0.66 for SC1 and SC3 data, respectively. To clarify the dependence, Figure 10d shows a plot of the electron temperature averaged over ion characteristic energy bins of width 100 eV. It is noteworthy that the functional relationships for the two spacecraft are the same, although there is significant time variability during their passage through the region. A linear fit to the combined data set from SC1 and SC3 yields a relationship $T_e = (0.7 \pm 0.1)E_c + (420 \pm 160)$.

[40] Straightforward energy, magnetic moment and flux conservation arguments lead to a well-known relationship between magnetospheric source electron temperatures and densities and the parallel potential along the field line [*Knight*, 1973], with $\Phi \sim T_e^{1/2}/n_e$. Such correspondences have been observed in lower altitude studies [e.g., *Burch et al.*, 1976; *Reiff et al.*, 1988; *Shiokawa et al.*, 2000]. Although we did not find a compelling density relationship, we tested independently for a dependence of ion characteristic energy (and hence for parallel potential) upon the square root electron temperature (Figures 10e and 10f). Comparisons with Figures 10b and 10c show that a root temperature dependence is not distinguishable from a linear dependence, although both are consistent with the data. (The limited dynamic range in the square root temperature comparison makes discrimination between the two difficult.) We stress that this behavior that is consistent with a Knight

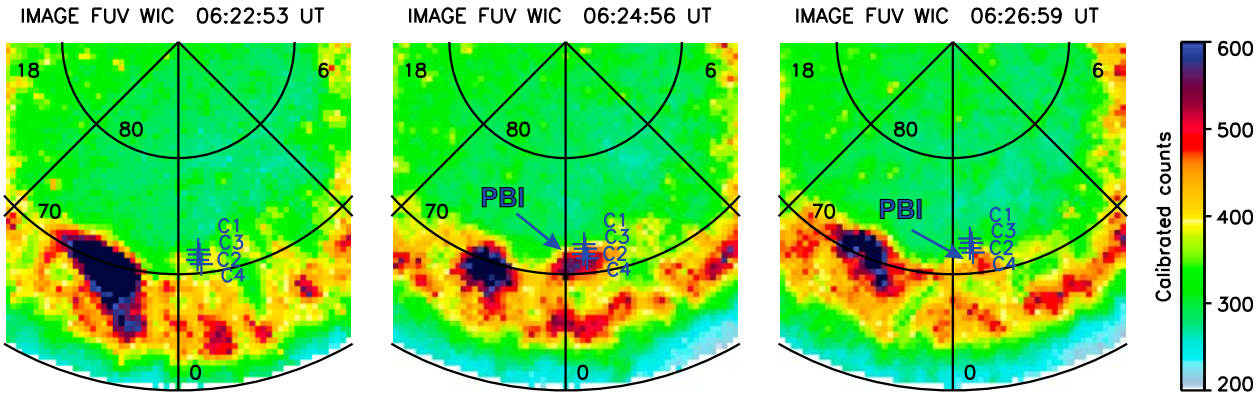

Figure 11. A sequence of auroral images sampled by FUV-WIC onboard IMAGE during and just after Cluster's traversal of the density cavity region. The foot point of the Cluster spacecraft are indicated by the crosses.

relation holds for a dynamic system. The variability here is on time scales comparable to an ion bounce period; to the electrons, therefore, the potential structures appear quasi static.

[41] The discussion above was focused on upward current regions. We note that there is also evidence of strong source electron temperature control of the time development of the parallel potential in downward current regions. This association is suggested by the following: 1) upgoing electron beams were observed to occur when the hot electrons were injected, and 2) the upgoing electron beam energy (a measure of the parallel potential below the spacecraft) increased with increases in the injected electron temperature. Analogous to upward current relationships, studies suggest the existence of a downward current-voltage relation in quasi-stationary downward current regions [e.g., *Temerin and Carlson*, 1998; *Cran-McGreehin and Wright*, 2005; *Hwang et al.*, 2009], which have qualitatively similar dependencies on source electron temperature. Namely, the equilibrium parallel potential drop is positively correlated with the magnetospheric electron temperature, all other things being equal. With evolution time scales long compared to the electron transit time, the observed trend noted here may be consistent with steady state expectations. However, a detailed evaluation of downward current-voltage models is in itself a separate topic, and is thus left as future work.

3.7. Auroral Emission Signatures

[42] To place these higher-altitude observations in context with auroral emissions, Figure 11 shows a sequentially sampled series of auroral images from the FUV-WIC instrument onboard the IMAGE spacecraft. The color table has been adjusted to exhibit clearly what are relatively weak emissions. The Cluster foot points mapped to the ionosphere using the Tsyganenko 1996 (T96) model (with observed input parameters Dst = −10, dynamic pressure 0.43 nPa, IMF By = +5, Bz = −1) are indicated with crosses. It is important to note that errors in the mapped foot points based on T96 and other models are not well known. The T96 model is an average model and does not take into account deflections from localized field-aligned currents and thus significant departures from a single event case study are possible. We found a 1° shift to the Cluster foot points yielded the most consistent agreement between image data and in situ measurements. We applied this shift in the comparisons shown in Figure 11.

[43] The first image (Figure 11 (left)) shows a relatively weak electron precipitation signature at the Cluster foot points. At this time, the lead spacecraft SC1 was in the center of a shallow cavity, whereas SC2–SC4 were located at or just before the cavity inner edge (see Figure 1a). No evidence of a sizable parallel potential was found in the ion data, consistent with the faint signature in the auroral image. Two minutes later in the subsequent image (Figure 11 (middle)) a localized auroral intensification was observed at the SC2 and SC4 foot points just equatorward of the polar cap. At this time, SC2 and SC4 were well within a much deeper cavity, whereas SC1 and SC3 had exited the cavity outer edge. The deeper cavity encompassed a pair of large-scale, upward and downward current sheets, both regions of which showed evidence that acceleration potentials had developed below Cluster. The sudden occurrence of the intensification in Figure 11 (middle) confirms our interpretation that a new quasistatic auroral arc current system formed in association with the expansion of the plasma sheet via an injection mediated process. The intensification is preferentially elongated in longitude, with the ratio of longitude to latitude widths being ~8 based on FWHM values. With Cluster's passage being near the center, the shape of the intensification is consistent with the determination of the large-scale current system geometry as a current sheet pair from timing and variance analysis. By the time the third image was sampled, all four Cluster spacecraft had exited the cavity and were in the polar cap, as the intensification slightly weakened, became thinner in latitude, and notably, drifted equatorward.

[44] The thickness (in latitude) and equatorward velocity of the intensification were determined using MLT cuts through the Cluster fleet foot points of the images shown in Figures 11 (middle) and 11 (right). Prior to computing these quantities, we applied a Gaussian fit to the intensification found in each invariant latitude count profile. Being above background levels, the intensification appearing in each of the MLT cuts (figure not shown) is easily identified for the purpose of the fits. From the FWHM of the Gaussian fit to the profile obtained from the image sampled at 0624:56 UT

(Figure 11 (middle)), the thickness of the intensification is estimated at ~260 km during the time the large-scale current system formed. The equatorward velocity is estimated to be 350 ± 140 m s^{-1} from the latitude displacement of the Gaussian peak of the fits to cuts from Figures 11 (middle) and 11 (right). For comparison, the thickness of the upward current part of the cavity mapped at ionospheric altitudes is determined to be 173 km (see section 3.3), which is consistent with the auroral emission estimate. In addition, the cavity normal velocity in an Earth fixed frame is found to be $V_{\mathrm{rel}}^{E} = V_{\mathrm{rel}} + \mathbf{V_{SC}} \cdot \hat{\mathbf{n}} = 4.3 \pm 1$ km s^{-1}. At ionospheric altitudes, this yields an arc system equatorward velocity of 500 ± 100 m s^{-1}, which is in good quantitative agreement with the auroral image estimate. The good agreement between the auroral emission and timing analysis estimates indicate that the equatorward velocity and thickness of the auroral intensification are seeded in structures occurring at and beyond Cluster's altitude as one may expect for large-scale arc systems. Not only does this result provide independent confirmation of the estimates obtained from the multispacecraft timing analysis applied to the higher altitude spacecraft potential measurements, it also establishes a direct correspondence between processes occurring at these higher altitudes that lead to auroral acceleration and ionospheric consequences.

4. Discussion

[45] The location, equatorward motion, and plasma injection characteristic of the poleward plasma sheet expansion suggest that the sequential observations shown here represent the high-altitude auroral zone counterpart of an auroral PBI, which have been observed at the poleward edge of the auroral oval in ground based radar and optical data, during geomagnetically quiet and active times [e.g., *de la Beaujardière et al.*, 1994; *Henderson et al.*, 1998; *Lyons et al.*, 2002; *Zesta et al.*, 2006, and references therein]. By inferences made from sequential ground based data and space-based global auroral images, PBIs are thought to be the result of the injection of plasma in the magnetotail, perhaps associated with a bursty patchy reconnection process, leading to the poleward expansion of the plasma sheet even as convection moves flux tubes equatorward. The multispacecraft results shown here provide strong evidence in support of such an injection mediated plasma sheet expansion scenario.

[46] The sequential observations from the Cluster spacecraft fleet shown here reveal how the properties of the plasma and fields change during the formation of an auroral arc system of a PBI at this high altitude location. Particularly noteworthy is that these changes manifest the development of a new quasi-static system of upward and downward current sheets with associated acceleration potential growth and density erosion out of an Alfvénic system of temporally evolving small-scale field aligned currents. In past single spacecraft based observational studies these systems were seen as distinct systems or perhaps in transition from one form to another. Here the multipoint observations show for the first time that quasi-static systems can form out of dynamic Alfvénic systems.

[47] The interpretation that the current system and associated parallel potentials evolved to a quasi-stationary state is based on the transformed properties of the electron and ion distribution functions and moments, and also on the structural changes in the current. We showed that the initial development of the arc system was associated with the appearance of quasi-periodic, small-scale current sheets superposed on a large scale FAC system threading through the PSBL. Small-scale currents, such as those documented here, are a common feature of the high-altitude PSBL and have been identified as being signatures of shear Alfvén waves generated from a magnetotail source [*Wygant et al.*, 2000; *Keiling et al.*, 2002]. Characteristic of the transformation shown here was the growth of a large-scale up-down current system accompanied by a sizable attenuation of the small-scale structure. Moreover, the electrons were shown to have less variability as they evolved to a loss cone distribution. In the upward current region we observed upgoing protons and electrons with field-opposed flux dropouts, signifying the development of a parallel potential below the spacecraft. Subsequent development of the upgoing protons to a beam with lower energy suggests that the potential relaxed as the system stabilized. Upgoing electrons were shown to occur in the downward current region with distribution spectra that were narrow in pitch angle and broad in energy. Such features are characteristic of the canonical quasi-static return current region and are attributed to upward acceleration through a thin potential layer followed by parallel heating via wave-particle processes. Together, these characteristics of the plasma and currents provide strong evidence that the system has evolved to a quasi-stationary arc system.

[48] It is unclear whether these evolutionary signatures are typical or a special class of the high-altitude auroral arc system formation process of PBIs. *Aikio et al.* [2008] reported an event observed by Cluster at the end of the substorm recovery phase associated with a sudden expansion (timescale of a few minutes) of the PSBL into the polar cap. In that event the electrons and accompanying currents and electric fields in the new extended region remain highly structured, with multiple occurrences of upward and downward current pairs with durations of a few tens of seconds similar to the small-scale fluctuations reported here. No large-scale upward and downward current sheet pair extending over the region, with attendant parallel potentials is apparent. Though the longer time development is uncertain, it may be the case that the signatures in the new PSBL region reported by *Aikio et al.* [2008] correspond to the early stages of the development of the large-scale arc system documented here. Indeed more events need to be examined to establish how such systems form and evolve.

[49] An understanding of the evolution seen in the Alfvénic field-aligned currents requires observations spaced along the geomagnetic field that are not available. The fact that the attenuation of these structures coincided with the merging of the injected hot tenuous electrons with the preexisting plasma sheet boundary layer population suggests that the injected plasma (particularly the electrons) may be playing a role in stabilizing the preexisting Alfvénic turbulence at the PSBL. This may be effected either by changing the magnetotail source conditions so as to preclude excitation, and/or by damping the small scale structure somewhere along the field line. Also in a self consistent manner, depending on whether these Alfvénic currents are transient or continuously

driven at the source, the dispersive Alfvén waves may be preconditioning these magnetospheric source electrons, which carry the current and hence can potentially influence parallel potential development (transient case) and stability (driven case) of the auroral acceleration region at lower altitude.

[50] Interestingly, the observed time sequence of the currents does have features that are qualitatively similar to the expectations of transient response models of magnetospheric-ionospheric coupling [e.g., *Nishida*, 1979; *Kan et al.*, 1982; *Baumjohann and Glaßmeier*, 1984]. Such models were developed to described large scale processes though are generalizable to smaller scale phenomenon at the PSBL presented here. In such models gross magnetospheric reconfigurations and associated sudden diversion of cross-tail current into a wedge current are communicated to the ionosphere via the launching of Alfvén waves. Owing to the impedance mismatch between magnetosphere and ionosphere, these Alfvén waves reverberate back and forth between these boundaries and ultimately damp out as the current system develops and comes to equilibrium. The damping of the Alfvénic transients in the models is achieved via joule dissipation in the ionosphere, which can take a few to several Alfvén wave bounce periods depending on the impedance mismatch. However, our observations indicate that the transverse scale size of these currents approached $2\pi\lambda_e$ as the cavity formed. In this limit parallel electric fields form and local dissipation through Landau damping [e.g., *Thompson and Lysak*, 1996] and/or quasi-static processes [e.g., *Wright et al.*, 2002] can occur. Such effects will influence, among other things, the relaxation time of the Alfvénic transients and thus such models will need to be modified to incorporate such effects for a more accurate description.

[51] We showed that the density cavity is predominantly due to the depletion of cold dense plasma of ionospheric origin with the injection of hot magnetospheric plasma. We view the depletion to be a consequence of parallel potential development in both the upward and downward current regions. In the upward current region, parallel electric fields developing below the spacecraft reflect upgoing cold, ionospheric electrons downward. At the same time, the cold ionospheric ion counterpart gets accelerated and rarefied to maintain current by the combined effects of the parallel potential and magnetic field. The density decrease in the downward current counterpart is, in part, likely due to a similar effect. The cold ionospheric electrons are accelerated and rarefied by the combined effects of the downward pointing parallel electric and magnetic fields, whereas the ions are prevented, in the absence of wave particle interactions, from attaining these higher altitudes as they are reflected by the potential.

[52] The shape of the cavity was asymmetric, with the density being measurably lower in the downward current region relative to its upward current counterpart. This is in contrast with localized density cavities that were observed by Cluster to form in association with parallel potentials at density gradients in downward current regions near or within the PSBL [*Marklund et al.*, 2004]. The differences between our event and those reported by *Marklund et al.* [2004] are likely related to whether or not cold plasma initially existed in the region. *Marklund et al.* [2004] suggested that the local cavity in the downward current region is related to density depletions in the ionosphere. Such depletions have been observed to form near the poleward edge of the most poleward auroral arc, during geomagnetic conditions that are quiet [e.g., *Doe et al.*, 1993, 1994] and more active [e.g., *Aikio et al.*, 2004]. However, we note that the cavity shown here is a remnant of plasma connected to both ionospheric and magnetospheric sources that are less dense than the cold plasma initially occurring in the region. Though the local depression in the downward current region in our event may be related to the development of a density depletion in the ionosphere, a significant factor is the more tenuous nature of the magnetospheric plasma connected to the downward current region.

[53] Theoretical [e.g., *Cran-McGreehin et al.*, 2007] and observational studies [*Marklund et al.*, 2001; *Aikio et al.*, 2004] indicate that the current system may broaden to access more current carriers to sustain a sufficiently large applied current as the ionospheric source for the current carriers get depleted in the nightside downward current region. We did not observe such an effect in our event, although the ionospheric mapped downward current amplitude is above the predicted threshold for broadening to occur [*Cran-McGreehin et al.*, 2007] and the system evolved over time scales similar to those encountered in other studies [*Marklund et al.*, 2001; *Aikio et al.*, 2004]. Either the electrons were accelerated by the parallel electric field to a sufficient velocity to carry the current or the finite ionospheric source may not be completely depleted (perhaps owing to the initially enhanced cold plasma density condition) in this case.

[54] We suggest that the cold dense plasma initially occupying the region where the cavity formed is the high-altitude manifestation of density enhancements called F region ionization patches observed in the polar cap ionosphere [e.g., *Buchau et al.*, 1983, 1985; *Robinson et al.*, 1985; *Weber et al.*, 1986]. Studies show that F region patches observed near the nightside polar cap boundary are not locally produced by soft electron precipitation or solar EUVE, but are enhancements of ionospheric plasma density via photoionization with origins within or equatorward of the cusp and which convect antisunward over the polar cap to the nightside polar cap boundary. If this interpretation is correct, then our example suggests that ionization patches influence the plasma conditions up to at least the altitudes sampled by Cluster. It remains to be shown whether or not arc systems which form at or near the PSBL under such enhanced density conditions are inherently different from those occurring in the absence of this population. The presence of a cold plasma population, whether it extends deep in the tail or has a limited altitude extent, is expected to influence the altitude and amplitude of the acceleration region potential drop that forms. This dense population can also affect the arc associated Alfvén wave communication from the magnetospheric generator to the ionosphere (and vice versa) such as in the propagation of phase fronts and phase mixing at the PSBL [e.g., *Semenov et al.*, 1999; *Wright et al.*, 1999]. Models describing such processes assume a sharp density gradient at the PSBL-polar cap transition, while our observations indicate the contrary.

[55] Finally, we note that the PBI shown in Figure 11 is not an isolated occurrence, but is one of a series of PBIs,

which recur and subsequently drift equatorward in sequential IMAGE data (not shown). The pulsations have an average cadence of ~13 minutes, which is in the Pc6 band. Thus the observed time sequence presented here and associated auroral intensifications may be an artifact of the excitation of a ULF mode deeper in the tail as suggested in past observations of PBIs [e.g., *Lyons et al.*, 2002; *Zesta et al.*, 2006].

5. Summary and Conclusions

[56] We have presented multipoint Cluster observations of the plasma and field properties at key instances during the formation of a new quasi-static auroral arc up-down current system. The quasi-static system evolved during relatively quiet magnetospheric conditions from an Alfvénic system of fine-scale, field-aligned currents at and just poleward of the plasma sheet boundary layer. The new arc system evolved in association with a local expansion of the plasma sheet. Key results documented in this paper are:

[57] 1. In previous single spacecraft studies the Alfvén wave dominated region and inverted V systems were seen as separate regions; multipoint Cluster observations demonstrate that quasi-static systems can form out of Alfvén dominated systems. The transition to an inverted V system was evidenced by the formation of a large-scale up-down, field-aligned current sheet pair system accompanied with a noticeable attenuation of the Alfvénic currents, and associated parallel potential development. Parallel potentials were signified by cavity formation, the cooccurrence of upgoing ion beams and modified loss cone electron distribution signatures in the upward current region, and upgoing electrons with distribution spectra that were narrow in pitch angle and broad in energy in the downward current region.

[58] 2. The Alfvénic currents have ionospheric values for the perpendicular widths and amplitudes ranging from 3–20 km and ~0.4–3.5 μA m^{-2}, respectively, and are associated with upgoing or counterstreaming electrons at energies from a 10s eV to 100s of eV. As the density cavity formed these Alfvénic currents became dispersive, with $2\pi\lambda_e/\lambda_\perp \rightarrow 1$, and hence perhaps attenuated via Landau damping near and above Cluster's altitude (e.g., within and above the high altitude acceleration region). The large-scale current sheet pair system was spatially asymmetric, with the upward current region being thicker (173 km) than its downward current counterpart (38 km), with peak amplitudes of 3.5 μA m^{-2} at ionospheric altitudes. This system formed after significant density depletion and signs of a parallel potential drop appeared. We did not observe significant broadening of the large-scale downward current region as density eroded therein. The ionospheric source may not yet be completely depleted in the downward current region and/or the potential was able to accelerate the electrons to a sufficient velocity to carry the current in this case.

[59] 3. The time sequence of the current is qualitatively consistent with the predictions of transient response models for magnetospheric-ionospheric coupling. However, our results suggest these models need to be modified to account for dissipation of sufficiently small-scale Alfvénic transients along the magnetic field.

[60] 4. Density cavitation was shown to be a consequence of an erosion of cold dense ionospheric plasma associated with the development of parallel potentials, as opposed to variations in the magnetospheric source electron density. We suggest this cold population may be the high-altitude manifestation of F region ionization patches. The cavity exhibited planar geometry, the location of transverse (with respect to **B**) boundaries of which were maintained as it deepened and moved equatorward at the convection velocity.

[61] 5. The upward current region potential inferred from upgoing ion characteristic energy initially formed under nearly constant macroscopic current conditions. We observed a reduction in the magnitude of this potential after it peaked, which indicates that the development process was nonmonotonic perhaps owing to a relaxation effect as the system stabilized. The upward current potential was correlated with the locally measured electron temperature. The temperature-potential correlation is consistent with a Knight-type dependence. The downward current potential inferred from upgoing electron energies increased in time coincident with an increase in the injected electron temperature. Although the current is of central importance in the occurrence of acceleration potentials, these results show strong magnetospheric electron temperature control of the upward and downward current region parallel potentials.

[62] 6. The process led to a PBI. The equatorward velocity and thickness of the PBI from IMAGE data are consistent with their ionospheric mapped cavity counterparts, suggesting that the motion and thickness are controlled by plasma and electrodynamic features at and above Cluster's altitude (~3.5 R_E).

[63] 7. The arc formation and consequent PBI were driven by the injection of a new hot, tenuous magnetospheric source population, and structure development led to local thickening of the plasma sheet, as this new hot population merged with the preexisting PSBL. Tail flapping or modulations due to large-scale surface waves are ruled out because this region is moving equatorward at the convection velocity as determined by multipoint measurements and confirmed in subsequent samples of auroral emission data from IMAGE.

[64] These temporal changes occurred on a time scale of a few minutes, which is on the order of Alfvén and acoustic wave transit times. This is also the characteristic time a 1 keV ion takes to transit from a near Earth source to Cluster's altitude.

[65] These results suggest the importance of magnetospheric plasma in driving the development of the auroral density cavity and acceleration potential. Irrespective of the mechanism, the injection of magnetospheric plasma near the PSBL appears to drive the development of the auroral arc system, including controlling the magnitude of the parallel potential, the depth of the density cavity that forms, and stabilization of the initial finely structured Alfvén dominated region preexisting just equatorward of the initial injection site.

[66] **Acknowledgments.** Partial support for this study was provided by NASA grants NAG5-12039, NNX07AG41G, NNG05GL27G. Partial support for C. Chaston was provided by grant ATM-0602728. We thank the FGM team and the Cluster Active Archive for the publicly available magnetic field data used in this study.

[67] Wolfgang Baumjohann thanks Kristina Lynch and Anita Aikio for their assistance in evaluating this paper.

References

Aikio, A. T., et al. (2004), Temporal evolution of two auroral arcs as measured by the Cluster satellite and coordinated ground-based instruments, *Ann. Geophys.*, *22*, 4089–4101.

Aikio, A. T., T. Pitkänen, D. Fontaine, I. Dandouras, O. Amm, A. Kozlov, A. Vaivads, and A. Fazakerley (2008), EISCAT and Cluster observations in the vicinity of the dynamical polar cap boundary, *Ann. Geophys.*, *26*, 87–105.

Andersson, L., R. E. Ergun, D. L. Newman, J. P. McFadden, C. W. Carlson, and Y.-J. Su (2002), Characteristics of parallel electric fields in the downward current region of the aurora, *Phys. Plasmas*, *9*(8), 3600–3609, doi:10.1063/1.1490134.

Balogh, A., et al. (1997), The Cluster magnetic field investigation, *Space Sci. Rev.*, *79*, 65–92.

Baumjohann, W., and K.-H. Glaßmeier (1984), The transient response mechanism and Pi2 pulsations at substorm onset—Review and outlook, *Planet. Space Sci.*, *32*(10), 1361–1370.

Bosqued, J. M. (1987), Aureol-3 results on ion precipitation, *Phys. Scr. T*, *18*, 158–161.

Buchau, J., B. W. Reinisch, E. J. Weber, and J. G. Moore (1983), Structure and dynamics of the winter polar cap F region, *Radio Sci.*, *18*, 995–1010.

Buchau, J., E. J. Weber, D. N. Anderson, H. C. Carlson Jr., J. G. Moore, B. W. Reinisch, and R. C. Livingston (1985), Ionospheric structures in the polar cap: Their origin and relation to 250-MHz scintillation, *Radio Sci.*, *20*, 325–338.

Burch, J. L., S. A. Fields, W. B. Hanson, R. A. Heelis, R. A. Hoffman, and R. W. Janetske (1976), Characteristics of auroral acceleration regions observed by Atmosphere Explorer C, *J. Geophys. Res.*, *81*, 2223–2230.

Cran-McGreehin, A. P., and A. N. Wright (2005), Current-voltage relationship in downward field-aligned current region, *J. Geophys. Res.*, *110*, A10S10, doi:10.1029/2004JA010870.

Cran-McGreehin, A. P., A. N. Wright, and A. W. Hood (2007), Ionospheric depletion in auroral downward currents, *J. Geophys. Res.*, *112*, A10309, doi:10.1029/2007JA012350.

Décréau, P. M. E., et al. (1997), WHISPER, a resonance sounder and wave analyser: Performances and perspectives for the Cluster mission, *Space Sci. Rev.*, *79*, 157–193.

de la Beaujardière, O., L. R. Lyons, J. M. Ruohoniemi, E. Friis-Christensen, C. Danielsen, F. J. Rich, and P. T. Newell (1994), Quiet-time intensifications along the poleward auroral boundary near midnight, *J. Geophys. Res.*, *99*(A1), 287–298.

Doe, R. A., M. Mendillo, J. F. Vickrey, L. J. Zanetti, and R. W. Eastes (1993), Observations of nightside auroral cavities, *J. Geophys. Res.*, *98* (A1), 293–310.

Doe, R. A., M. Mendillo, J. F. Vickrey, J. M. Ruohoniemi, and R. A. Greenwald (1994), Coordinated convection measurements in the vicinity of auroral cavities, *Radio Sci.*, *29*(1), 293–309.

Ergun, R. E., et al. (2001), Direct observations of localized parallel electric fields in a space plasma, *Phys. Rev. Lett.*, *87*, 045003.1–045003.4.

Gustafsson, G., et al. (1997), The electric field and wave experiment for the Cluster mission, *Space Sci. Rev.*, *79*, 137–156.

Harvey, C. C. (1998), Spatial gradients and the volumetric tensor, in *Analysis Methods for Multi-Spacecraft Data*, edited by G. Paschmann and P. W. Daly, pp. 307–322, Eur. Space Agency, Noordwijk, Netherlands.

Henderson, M. B., G. D. Reeves, and J. S. Murphree (1998), Are north–south aligned auroral structures an ionospheric manifestation of bursty bulk flows?, *Geophys. Res. Lett.*, *25*(19), 3737–3740.

Hwang, K.-J., K. A. Lynch, D. L. Newman, and C. W. Carlson (2009), FAST observations of downward current regions: Effect of magnetospheric conditions on the parallel potential drop, *J. Geophys. Res.*, *114*, A02218, doi:10.1029/2008JA013079.

Johnstone, A. D., et al. (1997), PEACE: A plasma electron and current experiment, *Space Sci. Rev.*, *79*, 351–398.

Kan, J. R., D. U. Longenecker, and J. V. Olson (1982), A transient response model of Pi 2 pulsations, *J. Geophys. Res.*, *87*(A9), 7483–7488.

Keiling, A., et al. (2002), Correlation of Alfvén poynting flux in the plasma sheet at 4–7 R_E with ionospheric electron energy flux, *J. Geophys. Res.*, *107*(A7), 1132, doi:10.1029/2001JA900140.

Kletzing, C. A., and J. D. Scudder (1999), Auroral-plasma sheet electron anisotropy, *Geophys. Res. Lett.*, *27*(7), 971–974.

Knight, S. (1973), Parallel electric fields, *Planet. Space Sci.*, *21*, 741–750.

Lyons, L. R., E. Zesta, Y. Xu, E. R. Sánchez, J. C. Samson, G. D. Reeves, J. M. Ruohoniemi, and J. B. Sigwarth (2002), Auroral poleward boundary intensifications and tail bursty flows: A manifestation of a large-scale ULF oscillation?, *J. Geophys. Res.*, *107*(A11), 1352, doi:10.1029/2001JA000242.

Marklund, G. T., et al. (2001), Temporal evolution of the electric field accelerating electrons away from the auroral ionosphere, *Nature*, *414*, 724–727.

Marklund, G. T., et al. (2004), Characteristics of quasi-static potential structures observed in the auroral return current region by Cluster, *Nonlinear Processes Geophys.*, *11*, 709–720.

McFadden, J. P., C. W. Carlson, and R. E. Ergun (1999), Microstructure of the auroral acceleration region as observed by FAST, *J. Geophys. Res.*, *104*, 14,453–14,480.

Mende, S. B., et al. (2000), Far ultraviolet imaging from the IMAGE spacecraft, *Space Sci. Rev.*, *91*, 243–318.

Mozer, F. S., and A. Hull (2001), Origin and geometry of upward parallel electric fields in the auroral acceleration region, *J. Geophys. Res.*, *106* (A4), 5763–5778.

Newell, P. T., Y. I. Feldstein, Y. I. Galperin, and C.-I. Meng (1996), Morphology of nightside precipitation, *J. Geophys. Res.*, *101*(A5), 10,737–10,748.

Newman, D. L., M. V. Goldman, R. E. Ergun, and A. Mangeney (2001), Formation of double layers and electron holes in a current-driven space plasma, *Phys. Rev. Lett.*, *87*(25), 255001.1–255001.4, doi:10.1103/PhysRevLett.87.255001.

Nishida, A. (1979), Possible origin of transient dusk-to-dawn electric field in the nightside magnetosphere, *J. Geophys. Res.*, *84*(A7), 3409–3412.

Paschmann, G., S. Haaland, and R. Treumann (Eds.) (2003), *Auroral Plasma Physics*, Kluwar Acad., Dordrecht, Netherlands.

Reiff, P. H., H. L. Collin, J. D. Craven, J. L. Burch, J. D. Winningham, E. G. Shelley, L. A. Frank, and M. A. Friedman (1988), Determination of auroral electrostatic potentials using high- and low-altitude particle distributions, *J. Geophys. Res.*, *93*(A7), 7441–7465.

Réme, H., et al. (1997), The Cluster ion spectrometry (CIS) experiment, *Space Sci. Rev.*, *79*, 303–350.

Robert, P., A. Roux, C. C. Harvey, M. W. Dunlop, P. W. Daly, and K.-H. Glassmeier (1998), Tetrahedron geometric factors, in *Analysis Methods for Multi-Spacecraft Data*, edited by G. Paschmann and P. W. Daly, pp. 323–348, Eur. Space Agency, Noordwijk, Netherlands.

Robinson, R. M., R. T. Tsunoda, J. F. Vickrey, and L. Guerin (1985), Sources of F region ionization enhancements in the nighttime auroral zone, *J. Geophys. Res.*, *90*(A8), 7533–7546.

Semenov, V. S., Y. B. Bogdanova, R. P. Rijnbeek, and M. J. Buchan (1999), A new mechanism for interpreting the motion of auroral arcs in the nightside ionosphere, *Geophys. Res. Lett.*, *26*(15), 2367–2370.

Shiokawa, K., W. Baumjohann, G. Haerendel, and H. Fukunishi (2000), High- and low-altitude observations of adiabatic parameters associated with auroral electron acceleration, *J. Geophys. Res.*, *105*(A2), 2541–2550.

Temerin, M., and C. W. Carlson (1998), Current-voltage relationship in the downward auroral current region, *Geophys. Res. Lett.*, *25*, 2365–2368.

Thompson, B. J., and R. L. Lysak (1996), Electron acceleration by inertial Alfvén waves, *J. Geophys. Res.*, *101*(A3), 5359–5369.

Weber, E. J., J. A. Klobuchar, J. Buchau, H. C. Carlson Jr., R. C. Livingston, O. de la Beaujardiere, M. McCready, J. G. Moore, and G. J. Bishop (1986), Polar cap F layer patches: Structure and dynamics, *J. Geophys. Res.*, *91*, 12,121–12,129.

Wright, A. N., W. Allan, R. D. Elphinstone, and L. L. Cogger (1999), Phase mixing and phase motion of Alfvén waves on tail-like and dipole-like magnetic field lines, *J. Geophys. Res.*, *104*(A5), 10,159–10,175.

Wright, A. N., W. Allan, M. S. Ruderman, and R. C. Elphic (2002), The dynamics of current carriers in standing Alfvén waves: Parallel electric fields in the auroral acceleration region, *J. Geophys. Res.*, *107*(A7), 1120, doi:10.1029/2001JA900168.

Wygant, J. R., et al. (2000), Polar spacecraft based comparisons of intense electric fields and poynting flux near and within the plasma sheet-tail lobe boundary to UVI images: An energy source for the aurora, *J. Geophys. Res.*, *105*, 18,675–18,692.

Zelenyi, L. M., R. A. Kovrazhin, and J. M. Bosqued (1990), Velocity-dispersed ion beams in the nightside auroral zone: AUREOL3 observations, *J. Geophys. Res.*, *95*, 12,119–12,139.

Zesta, E., L. Lyons, C.-P. Wang, E. Donovan, H. Frey, and T. Nagai (2006), Auroral poleward boundary intensifications (PBIs): Their two-dimensional structure and associated dynamics in the plasma sheet, *J. Geophys. Res.*, *111*, A05201, doi:10.1029/2004JA010640.

J. W. Bonnell, C. C. Chaston, M. Fillingim, A. J. Hull, J. P. McFadden, F. S. Mozer, and M. Wilber, Space Sciences Laboratory, University of California, Berkeley, CA 94720, USA. (ahull@ssl.berkeley.edu)

M. L. Goldstein, NASA Goddard Space Flight Center, Mail Code 673, Greenbelt, MD 20771, USA.